Preparation of Silicon Nanowires Photocathode for Photoelectrochemical Water Splitting

Zainab K. Ali[1a*], Mazin A. Mahdi[1b]

[1]*Department of Physics, College of Science, University of Basrah, Basrah, Iraq.*
[a]E-mail: kadhimzainab208@gmail.com
[b*]Corresponding author: m.a.mahdi@uobasrah.edu.iq

Abstract

A metal-assisted chemical etching process employing p-type silicon wafers with varied etching durations is used to produce silicon nanowires. Silver nanoparticles prepared by chemical deposition are utilized as a catalyst in the formation of silicon nanowires. Images from field emission scanning electron microscopy confirmed that the diameter of SiNWs grows when the etching duration is increased. The photoelectrochemical cell's characteristics were investigated using p-type silicon nanowires as working electrodes. Linear sweep voltammetry (J-V) measurements on p-SiNWs confirmed that photocurrent density rose from 0.20 mA cm^{-2} to 0.92 mA cm^{-2} as the etching duration of prepared SiNWs increased from 15 to 30 min. The conversion efficiency (η) was 0.47 for p-SiNWs prepared with a 15-minute etching time and 0.75 for p-SiNWs prepared with a 30-minute etching time. The cyclic voltammetry (CV) experiments performed at various scan rates validated the faradic behavior of p-SiNWS prepared for 15 and 30 min of etching. Because of the slow ion diffusion and the increased scanning rate, the capacitance decreased with increasing scanning rate. Mott-Schottky (M-S) investigation showed a significant carriers concentration of 3.66×10^{20} cm^{-3}. According to the results of electrochemical impedance spectroscopy (EIS), the SiNWs photocathode prepared by etching for 30 min had a charge transfer resistance of 25.27 Ω, which is low enough to enhance interfacial charge transfer.

1. Introduction

Providing sufficient energy for the world's population to achieve the required level of life is one of the most serious challenges facing humanity in the twenty-first century. The present world's population of 7 billion consumes 15 terawatts of energy; by 2050, this figure is projected to increase to 9 billion and 30 terawatts [1]. Approximately 80% of our energy demands are now supplied by fossil fuels, which will not be sufficient to satisfy global energy demand [2]. In addition, the use of fossil fuels has continued to increase during the past decade, and this trend is expected to continue over the next decade [3]. With the help of solar energy, photoelectrochemical (PEC) water splitting is one of the most common techniques for producing hydrogen fuel, which can replace traditional fossil fuels in next-generation renewable energy applications. A solar-assisted PEC system is often associated with the conversion of solar energy into electrical energy via a semiconductors/electrolyte interface. When photons with energy higher than the bandgap of a semiconductor are absorbed, electron-hole pairs are produced, which are separated when the electrons are transferred from the valence band to the conduction band. In addition, the appropriate energy positioning of the bands causes a water molecule in contact with semiconductors to be reduced to H_2 by photoelectron and oxidized to O_2 by photo holes [4-6].

Several critical parameters must be achieved simultaneously for direct photoelectrochemical water splitting to occur efficiently and sustainably. When irradiated, the semiconductor system must produce enough voltage to split water, and the semiconductor band gap must be small enough to absorb most of the sunlight; at the surface, the band edge potentials must intersect the hydrogen and oxygen redox potentials, and the system [7]. Therefore, efficient photocathodes based on combination of semiconductors as a catalyst is required to hydrogen evolution reaction (HER) [8]. The photoelectrochemical (PEC) water splitting method employing semiconductor materials has grown in popularity as one of the clean, environmentally friendly, and low-cost solutions to the energy issue [9, 10]. Suitable photoelectrodes for PEC water splitting are cadmium selenides (band gap 1.7 eV), cadmium sulphides (band gap 2.4 eV), titanium dioxide (band gap 3.0 eV) and silicon (band gap 1.1 eV) [11-14]. Silicon is the perfect photoelectrode because of its low bandgap. Si with a narrow bandgap absorbs most of visible light and has a comparatively high electrolyte corrosion stability. The edge of its conduction band is well above $E0(H+/H_2)$. Si would therefore be a suitable photocathode material for the hydrogen evolution process (HER) [15]. Furthermore, one-dimensional silicon nanowires (Si NWs) exhibit superior conductivity in the PEC water splitting process compared to bulk silicon due to their faster charge transport track, more effective charge collection, greater contact area with the electrolyte, and reduced reflection [16]. Enhancing the efficacy of PEC water splitting requires increasing the diameters of Si nanostructures, which enhances active sites at the semiconductor/electrolyte interface. Even in the absence of a co-catalyst, the diameter of NWs and their surface shape have been proven to be important parameters for an efficient photoelectrode that increases the overall PEC water splitting process [15, 16]. In the present work, p-SiNWs photoelectrode were fabricated by the two-step metal-assisted chemical etching (MACE) method using a p-Si (100) substrate. The PEC water splitting was investigated by studying cyclic voltammetry, current density, electrochemical impedance spectroscopy (EIS) of the working electrode/electrolyte interface, and Mott-Schottky (M-S) values for measuring internal electronic properties of the working electrode and hydrogen gas evolution occurring throughout the process.

2. Experimental work
2.1. Preparation SiNWs using MACE Method

Polished p-type Si(100) wafers with a resistivity of 1-10 Ω.cm were used to prepare the silicon nanowires (SiNWs) using the metal-assisted chemical etching (MACE) approach.

Before the etching process, the Si wafer was cut into small pieces of 1×1.5 cm. Then, the Si wafers were cleaned by immersing them in a beaker containing distilled water (DW) for 10 min in an ultrasound bath. Then, Si wafers were washed using acetone and ethanol under sonication, and finally they were washed with DW. The SiO_2 thin layer is finally removed from the surface by dipping the Si(100) wafers in 5% diluted HF acid for 1 min. Si(100) substrates were placed into a solution containing 0.06 mol/L of $AgNO_3$ and 5M of HF for 30 seconds to deposit Ag nanoparticles on the surface, and then SiNWs were grown on them as a catalyst using Ag nanoparticles. The prepared Si(100) wafers Ag NPs coated were immersed in a solution of 2M H_2O_2 and 5M HF at room temperature to grow SiNWs with different etching times of 15 and 30min. After the etching process was complete, the samples were washed with DW and immersed for 30 seconds in a diluted HNO_3 solution to

remove the Ag particles deposited on the surface of the SiNWs [17]. Fig. 1 depicts the preparation steps for SiNWs.
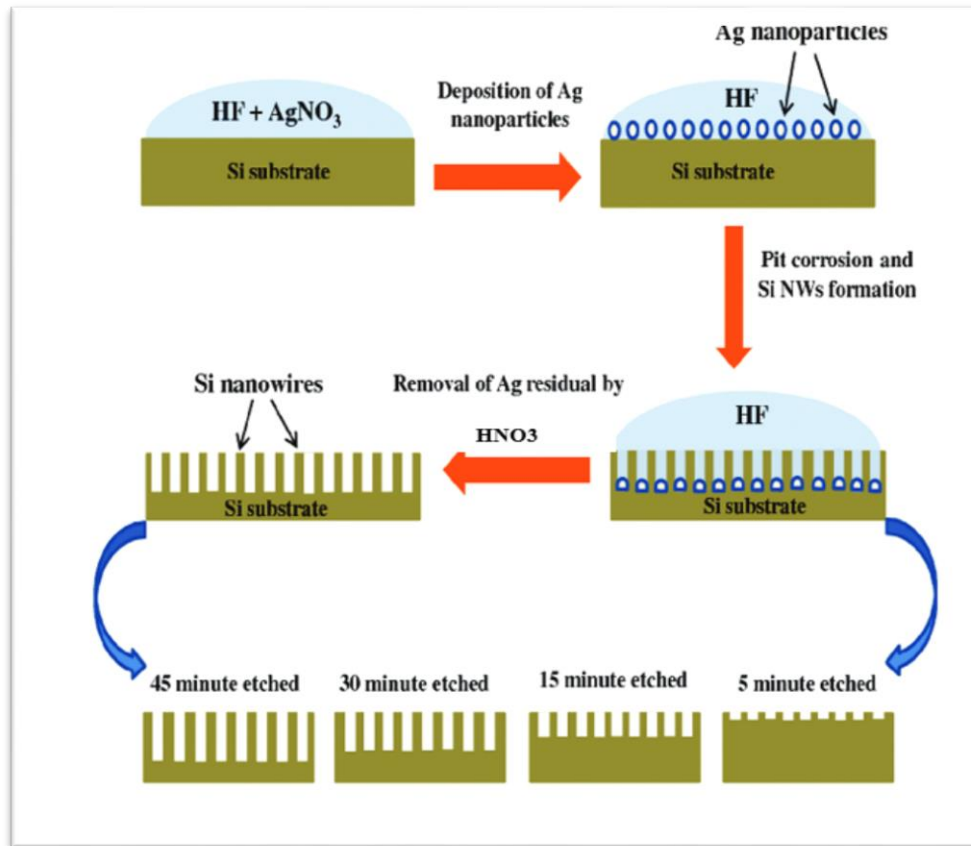

Figure 1: A diagram illustrating the production of NWs through metal-assisted chemical etching (MACE) process.

2.2. PEC Measurements

Ohmic contact electrodes were done by depositing aluminum (Al) metal on the back surface of the grown samples by thermal evaporation method and the back of the sample was connected to a copper wire using silver paint. The backside and edges of the samples were coated with epoxy, and the copper wire was enclosed in plastic tubes to isolate the electrical contacts from the electrolyte allowing the front side of the sample to come into contact with the electrolyte. The PEC tests were carried out in a quartz electrochemical cell with a corrTest electrochemical workstation in a standard three-electrode setup; the prepared samples served as the working electrodes, a platinum plate (1x1 cm) served as a counter electrode, while the Ag/AgCl electrode served as the reference electrode. The molarity of the electrolyte was 0.5 M Na_2SO_4 solution, and the pH of the electrolyte was 8.62.

Solar illumination with a power of 100 mW/cm^2 was employed as a light source to illuminate the surface of the samples. Using the Nernst equation, the measured potential versus Ag/AgCl was converted to the reversible hydrogen electrode

$$(RHE). E_{RHE} = E_{Ag/AgCl} + 0.059pH + E^o_{Ag/AgCl} \qquad\qquad (1)$$

In this case, ERHE stands for the converted potential vs RHE, $E^o_{Ag/AgCl}$ which is equal to 0.1976 V at RT, and $E^o_{Ag/AgCl}$ is the empirically observed potential vs the reference of Ag/AgCl, as well as the pH of the electrolyte solution in the PEC cell.

2.2.1. Electrochemical Performance Measurement

The performance of the PEC cell was evaluated using a variety of tests, such as Cyclic Voltammetry (CV) experiment, which was carried out six times under dark conditions using a scan rate of 50, 100, 200, 300, 400, and 500 mV/s. The negative and positive potential windows were -1.1 V to +1.1 V vs Ag/AgCl. Linear Sweep Voltammetry (LSV) was carried out with a scan rate of 500 mV/s under both dark and solar illumination conditions. The scan rate was configured for the photocathode to be 500 mV/s from -1.2 to 0 V vs Ag/AgCl. The photoconversion efficiency (η) was calculated based on the relationship:

$$\eta = |J_{pc}| \times \left(\frac{1.23 - V_b}{P_{\text{light}}}\right) \times 100 \tag{2}$$

where: J_{pc}, V_b, and P_{light} are photocurrent density (mA. cm^{-2}), the applied bias potential versus hydrogen reference electrode, and the illumination light intensity (mW.cm^{-2}), respectively.

2.2.2. Mott-Schottky Measurement

The Mott–Schottky measurements under dark conditions are done to determine the charge carriers' density (N_A) and the flat band potential (V_{FB}) for the photoelectrodes. Mott–Schottky theory is used to analysis the interfacial capacitance of the semiconductor/electrolyte junction through the following equation [18]:

$$\frac{1}{C_{Sc}^2} = \frac{-2}{\varepsilon_r \varepsilon_0 A^2 e N_A} \left(V - V_{fb} - \frac{kT}{e}\right) \tag{3}$$

where: C, ε_0, ε_r A^2, e, V, K, T are the space charge capacitance (F/cm^2), the vacuum permittivity (8.854 x 10^{-14} F/cm), the dielectric constant of the semiconductor (11.7 for Si), the electron charge (1.6 x 10^{-19} C), applied potential, Boltzmann constant (1.38 x 10^{-23} J/K), and the temperature, respectively [19]. The N_A was calculated using the slope of the Mott– Schottky (M-S) curve using the equation:

$$N_A = \frac{2}{\varepsilon_r \varepsilon_0 e S} \tag{4}$$

where: S is the slope of the M-S plot. Furthermore, the flat-band potential can be calculated by extrapolating the M-S plot to the x-axis intersection. At the intersection, the following relationship is used to obtain the flat-band potential [20]:

$$V_{fb} = V - \frac{k_B T}{e} \tag{5}$$

2.2.3. Electrochemical Impedance Spectroscopy (EIS)

The Electrochemical Impedance Spectroscopy (EIS) was carried out to determine the electrical characteristics of the Si wafer and SiNWs photocathodes prepared by etching for 15- and 30-min. EIS was calculated under dark and solar illumination for all electrodes. The AC voltage capacitance was 0.01V and the frequency range was 10^5 Hz - 0.1 Hz.

3. Results and Discussion

3.1. Morphology and Optical Properties

Fig. 3 shows the FESEM images of the SiNWs surface prepared using different etching times. The diameter of the prepared SiNWs prepared with 15 min etching

time was in the range of 26-304 nm. Whereas increasing the etching time to 30 min led to an increase in the diameter of the prepared SiNWs to 53-320nm. The increase in the the grown wires diameter with the increase in the etching time could be due to NWs being conglomerated together. Rai et al. prepared SiNWs via two-step MACE using Ag NPs as catalysts using different etching times of 10, 20, and 30 s, and found that the diameters of the deposited SiNWs were 63.94, 55.05, and 88.16 nm, respectively [21].
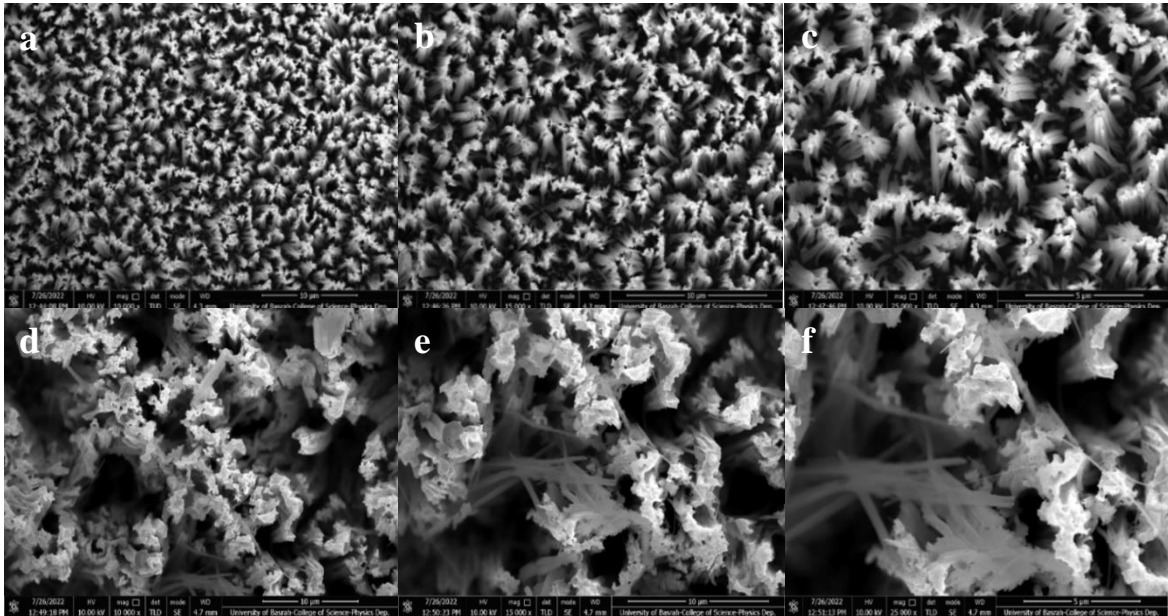

Figure 2: FESEM images of p-SiNWs grown etching time of (a) (Mag. = 10.000 K X), (b) (Mag. = 15.000 K X) and (c) (Mag. = 25.000 K X) for 15 min., (d) (Mag. = 10.000 K X) (e) (Mag. = 15.000 K X), and (f) (Mag. = 25.000 K X) for 30 min.

3.2. Photoelectrochemical Properties

Fig. 3a shows linear sweep voltammetry (J-V) curves of the p-Si(100) wafer photocathode in the dark and under solar illumination. A low current was observed in the dark, while the photocurrent density under -1.2 V bias voltage was -0.16 $mA.cm^{-2}$ under solar illumination. The photocurrent density was low under solar illumination which is due to the recombination of photo-induced charge carriers. Fig. 3b shows linear sweep voltammetry (J-V) curves of the p-SiNWs photocathode prepared by etching for 15 min in the dark and under solar illumination. A low current was observed in the dark while the photocurrent density under -1.2 V bias voltage was -0.20 $mA\ cm^{-2}$ under solar illumination. Fig. 3c shows linear sweep voltammetry (J-V) curves of the p-SiNWs photocathode prepared by etching for 30 min in the dark and under illumination. A low current value was observed in the dark while the photocurrent density with -1.2 V bias voltage was -0.92 $mA\ cm^{-2}$ under solar illumination.
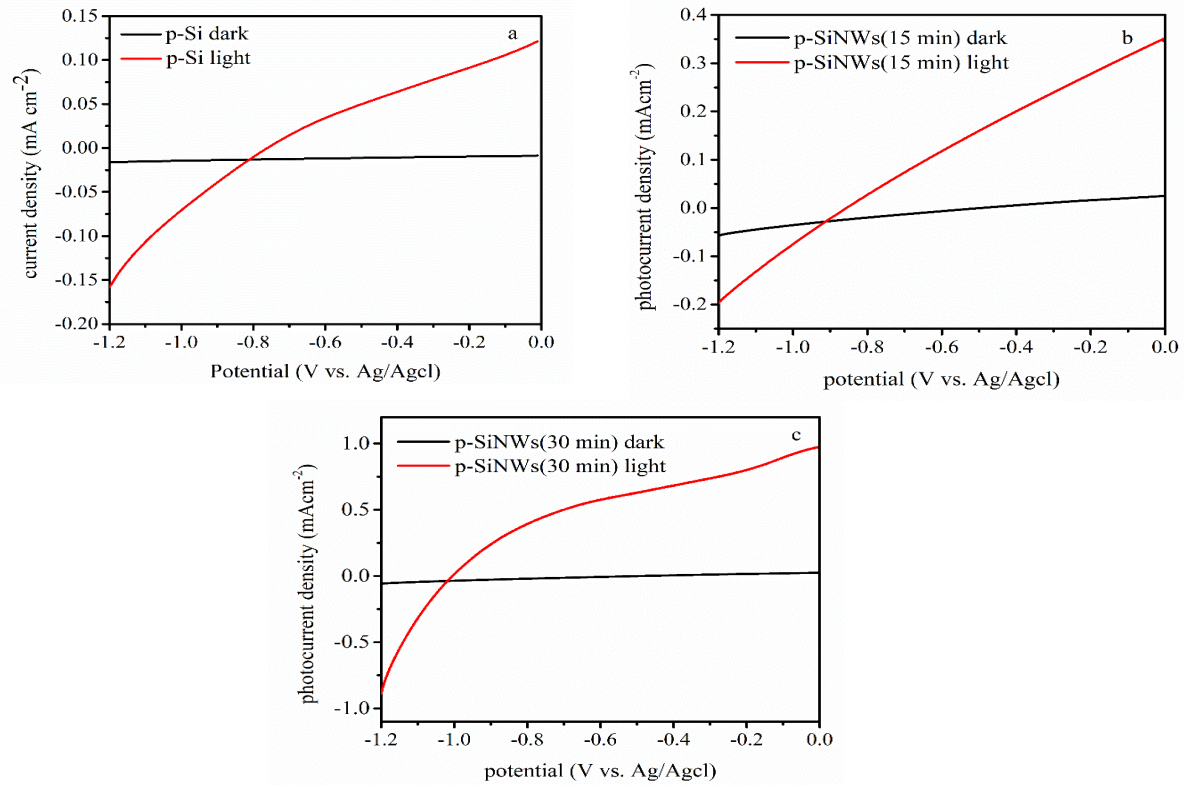
Figure 3: Linear sweep voltammetry (J-V) of Si (100) wafer photocathode and SiNWs photocathode prepared by etching time of 15 min and 30 under dark and light conditions.

Fig. 4 shows the η of the p-Si(100) wafer and p-SiNWs prepared with etching for 15 min 30 min. High value of η was 0.75% at a potential of -0.23V was obtained for the p-SiNWs prepared with 30min of etching time, while the samples prepared with 15min had η of 0.47% at a potential of -0.32V. However, the maximum value of η for p-Si (100) wafer was 0.1% obtained at a potential of -0.34V. The value of η was increased by 7.5 times for SiNWs prepared with an etching time of 30min and 4.7 times for samples prepared with 15min of etching time. These results agreed with the results of previous research, as shown in Table 1, under solar illumination.
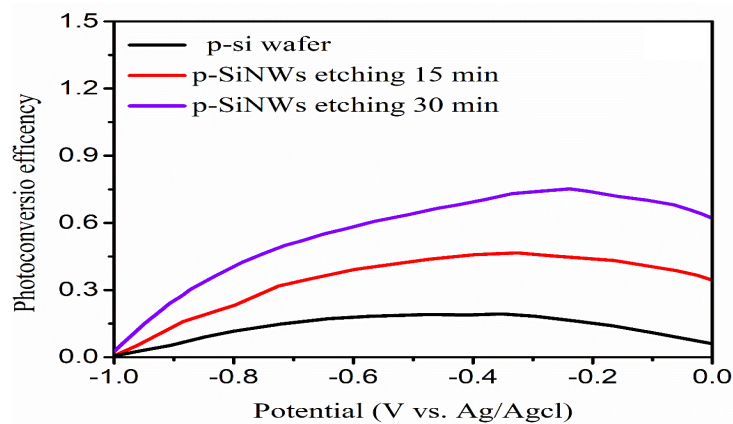

Figure 4: Photoconversion efficiency (η) as a function of potential for Si (100) wafer, and SiNWs prepared using 15min and 30min of etching time.

71

Table 1: Photoconversion efficiency(η) of prepared SiNWs using different durations compared with previous works

Photoelectrode	electrolyte	Con. (M)	P (mW/cm^2)	η%	V$_{Bais}$ (v)	Ref.
P-Si	H_2SO_4	0.5	100	0.1	0.80	[8]
P-SiNW	H_2SO_4	0.5	100	0.23	0.80	[8]
P-Si	$HClO_4$	1	100	0.03		[22]
P-Si	$HClO_4$	1	100	0.02		[23]
P-SiNW	$HClO_4$	1	100	0.91		[23]
P-SiNW	Na_2SO_4	0.5	100	1.1	0.78	[24]
P-Si	Na_2SO_4	0.5	100	0.1	-0.34	This work
P-SiNW etching 15min	Na_2SO_4	0.5	100	0.47	-0.32	This work
P-SiNW etching 30min	Na_2SO_4	0.5	100	0.75	-0.23	This work

The cyclic voltammetry (CV) measurements under dark were repeated 6 times using different scan rates of 50, 100, 200, 300, 400, and 500 mv/s for one cycle. Fig. 5a shows the CV curves for the Si wafer photocathode with different scan rates. The CV curve of pristine p-Si electrode shows a quasi-rectangular behavior and symmetrically shaped curve without redox peaks that infer that the capacitance is stored by an accumulation of charges between the electrode/electrolyte interfaces, indicating the electrical double layer capacitive behavior [25]. However, the area of CV curves and the value of the current increased with the scan rate, which indicates rapid charge–discharge reversibility. Fig. 5b shows the CV curves for the SiNWs photocathode prepared by etching for 15 min with different scan rates. The CV curve of the SiNWs electrode shows symmetric behavior with the appearance of oxidation peak, indicating the presence of faradic behavior leading to pseudocapacitance and electric double-layer capacitance [26]. However, under 50, 100, 300, 400, and 500 mV/s, the curves exhibited anodic peaks nearest from -0.14 V vs Ag/AgCl in the negative potential. Fig. 5c shows the CV curves for the SiNWs photocathode prepared by etching for 30 min with different scan rates. The CV curve of the SiNWs electrode shows asymmetric behavior with a reduction peak, indicating the presence of faradic behavior. However, under 400 and 500 mV/s, the curves exhibited anodic peaks nearest from -0.12 V vs Ag/AgCl in the negative potential.

The areal capacitance is calculated according to the following equation [27]:

$$C_s = \frac{1}{2sv\Delta v} \int I dv \qquad (6)$$

Where: C_s , $\int I dv$, s, v, Δv are the specific capacity (F/cm^2), the area under the curve, area of the electrode surface, scan rate, and potential window of the electrolyte, respectively.
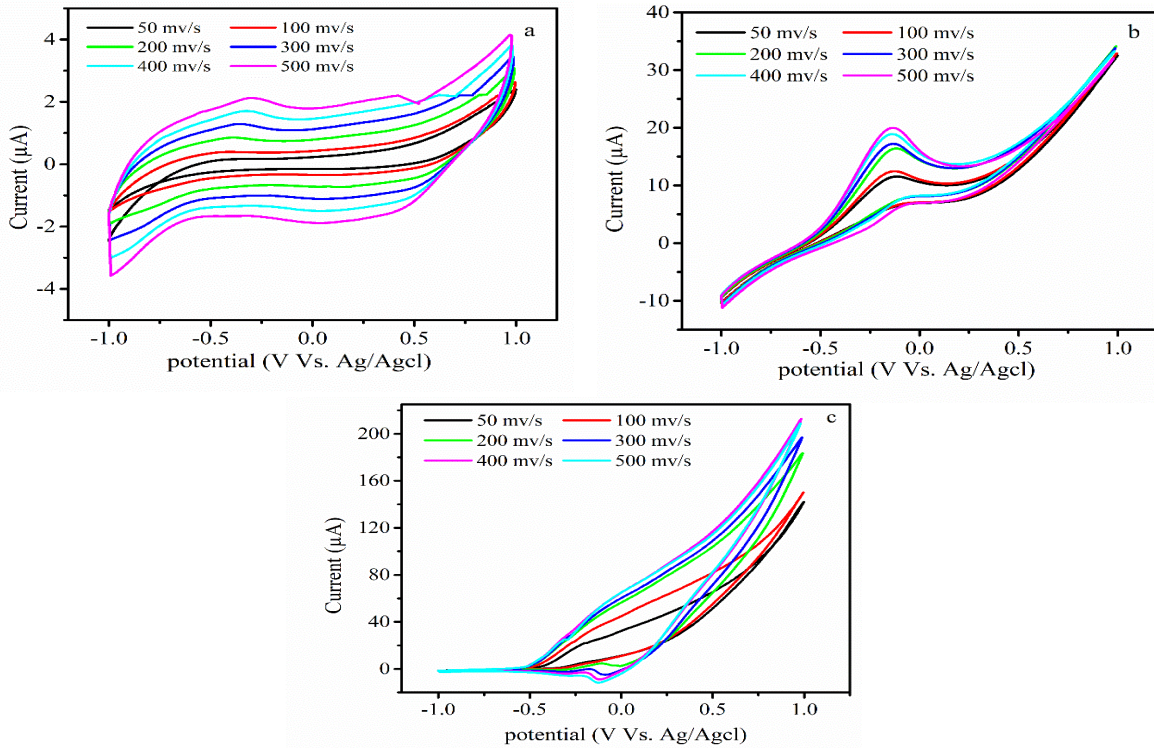
Figure 5: Cyclic voltammetry (cv) of (a) the Si(100) wafer photocathode, (b) SiNWs photocathode prepared by etching for 15 min, and (c) the SiNWs photocathode prepared by etching for 30 min.

Fig. 6 shows the areal capacitance reduction with scan rate values increasing from 50 to 500 mv/s for p-Si wafer and for p-SiNWs etched for15 min and 30 min. The maximum specific capacitance (Cs) was achieved at a scan rate of 50 mv/s, while for p-Si wafer, it was 2.6 μF/cm^2 and for p-SiNWs etched for 15 min, and 30 min were 13.3 μF/cm^2 and 60.06 μF/cm^2, respectively.

Increasing the scan rate produces a fast decrease in the concentration of electrical ions on the electrode surface. Additionally, the area of the lower surface of the electrode is involved in electrochemical processes at a fast scan rate. This means that the area of the inner surface of the electrode plays a significant part in this process [28].
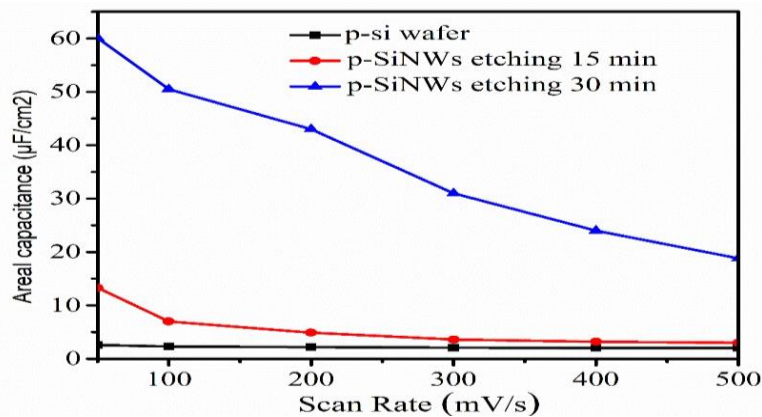

Figure 6: Areal capacitance of p-Si wafer, p- SiNWs etching 15 min, and p-SiNWs etching 30 min.

Mott–Schottky (M-S) measurements of Si(100) wafer and SiNWs electrodes prepared with etching times of 15 min and 30 min were carried out using different frequencies of 100, 1000, and 10000 HZ. The results of the M-S measurements are shown in Figs. 7,8 and 9, where the M-S Equation 3 is plotted as a function of the applied bias voltage. Fig. 7a-c shows M-S measurements of p-Si(100) wafer and SiNWs photocathode prepared with etching times of 15 and 30min under a frequency of 100 Hz.   The flat band potential (V_{FB}) was determined by projecting the interception of the straight line to the axis of applied potential. The V_{FB} values were 0.73 ,0.46, and 0.24V for p-Si(100) wafer, SiNWs photocathode prepared with an etching time of 15 min and those prepared with etching time of 30 min, respectively. These obtained values of VFB are in good agreement with that those of Meng et al. their VFB was 0.24 [29].

The acceptor density (N_A) of p-Si(100), SiNWs photocathode prepared with 15min and 30min of etching time were 5.88×10^{17}, 2.53×10^{19}, 3.66×10^{20}cm^{-3}, respectively. Qiao et al. [30] found N_A equal $5.52x10^{21}$ cm^{-3} for p-SiNWs prepared by Metal catalyzed electroless etching (MCEE). Further, the negative Mott-Schottky slope indicates that the semiconductor is p-type [31].
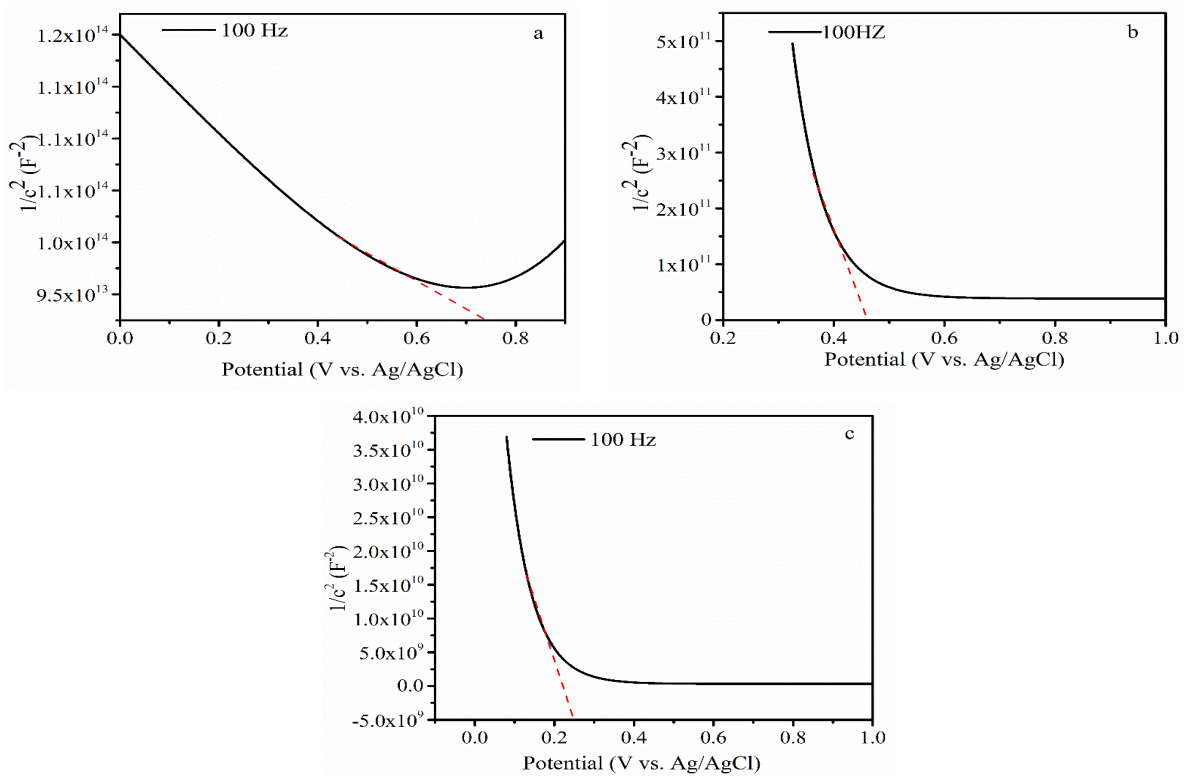

Figure 7: Mott-Schottky plots at frequency of 100Hz in the dark of the (a) p-Si(100), (b) SiNWs photocathode prepared by etching time of 15 min and (c) SiNWs photocathode prepared by etching 30 min.

Figs. 8a-c shows M-S measurements of p-Si(100) wafer and SiNWs photocathode prepared with etching times of 15 and 30min under a frequency of 1000 Hz. The V_{FB} values were 0.67, 0.44, and 0.23V for p-Si(100) wafer, SiNWs photocathode prepared with an etching time of 15 min, and 30 min, respectively. The N_A of P-Si(100), SiNWs photocathode prepared using 15min and 30min of etching time were 5.8×10^{17}, 1.27×10^{19}, 1.22×10^{20}cm^{-3}, respectively.
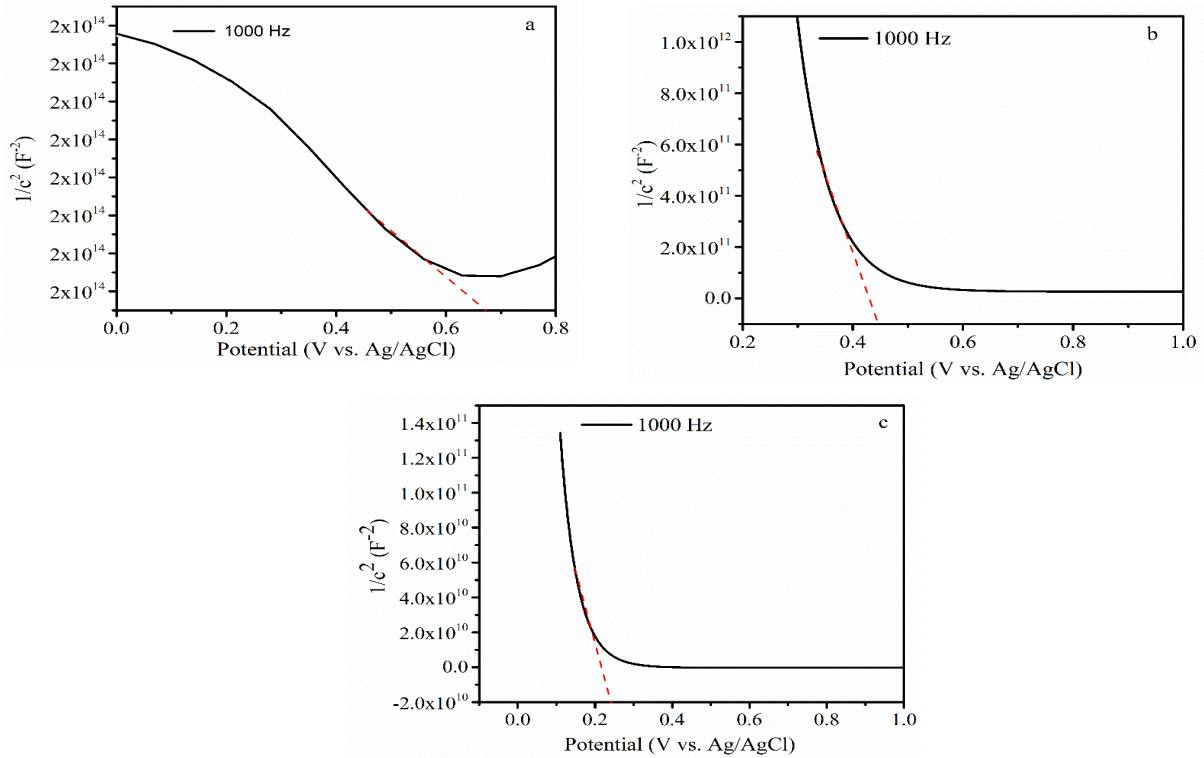
Figure 8: Mott-Schottky plots at a frequency of 1000 Hz in the dark of the (a) p-Si(100), (b) SiNWs photocathode prepared by etching 15 min, and (c) SiNWs photocathode prepared by etching 30 min.

Figs. 9 a-c shows M-S measurements under a frequency of 10000 Hz for p-Si(100) wafer and SiNWs photocathode prepared with etching times of 15 and 30min. The V_{FB} values were 0.59, 0.44, and 0.23V for p-Si(100) wafer and SiNWs photocathode prepared with etching times of 15 min, and 30 min, respectively. The N_A of p-Si(100) and SiNWs photocathode prepared with 15min and 30min etching times were 1.4×10^{17}, 6.28×10^{18}, 1.02×10^{20} cm^{-3}, respectively.

The Mott–Schottky results confirmed the capacitance decreased with increasing frequency, while as frequency increased, the flat-band potential decreased. This decrease is attributed to the wide band gap of the SiNWs structures compared to Si(100) wafer [32]. All values of V_{FB} were less positive for the prepared SiNWs indicating better performance of the photocathode electrode in capturing and rapidly transferring photogenerated electrons between the semiconductor and electrolyte interfaces [30]. The N_A value decreased when the frequency was increased for all samples. SiNWs photocathode prepared with 30 min etching time has the highest carrier concentration, which improves electronic conductivity and results in faster charge transfer [36]. The high value of N_A could be referred to the increase the hydrogen vacancies inside the crystalline structure formed at deposition nanowires (NWs) and which act as a hole acceptor. However, higher values of N_A at low frequencies refers to some contribution from surface states of capacitance data as pointed by Riveros et al. [33].
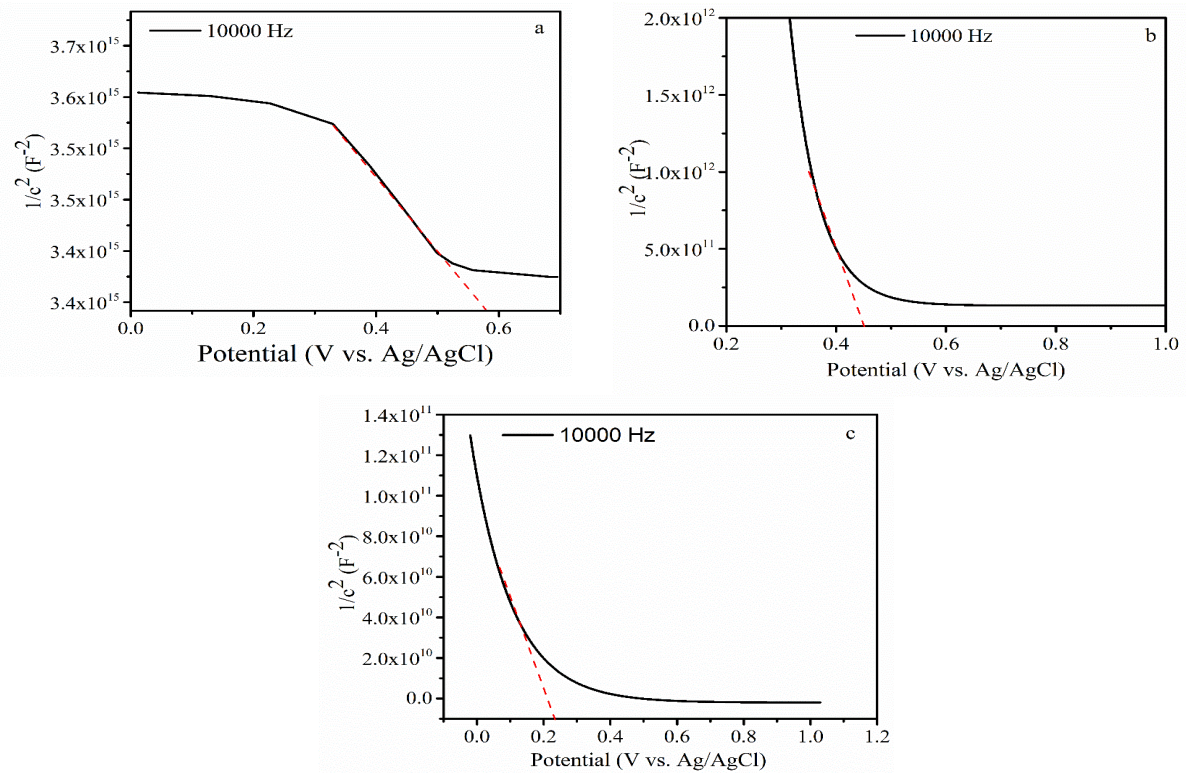
Figure 9: Mott-Schottky at a frequency of 10000 Hz in the dark plots of the (a) p-Si(100), (b) SiNWs photocathode prepared by etching 15 min, and (c) SiNWs photocathode prepared by etching 30 min.

The electrochemical impedance spectra (Nyquist plot) p-Si(100) wafer and p-SiNWs electrodes prepared with etching times of 15 min and 30 min are shown in Fig. 10. Fig. 10a depicts the Nyquist plot for the p-Si(100) wafer under solar illumination and in the dark. Fig. 10b shows a magnification for high-frequency region (0-200 Ω). The spectrum displays two semicircular arcs in the high- and low-frequency regions. The intercept of the linear portion on the real axis (Z') indicates equivalent series resistance (R_s), which reflects the overall series resistance combining electrolyte solution resistance and electrode internal resistance. The determined Rs for the p-Si(100) wafer was 16.8Ω. However, the diameter of semicircular arc located at the middle section of z' axis indicates that the charge transfer resistance (R_{ct}) of the electrode was 136.8 Ω. At high- frequency region, the appearance of a large semi-circle was noted indicating slower transfer of charges, where the first semi-circle arc at high frequency of 100 kHz corresponds to the process of charge-transfer resistance ($R_{ct.sc}$) process in the depletion layer of the semiconductors (working electrode), while the second semi-circle in the low-frequency corresponds to the charge transfer resistance ($R_{ct.dl}$) between the working electrode/electrolyte interface. This resistance is attributed to charge transfer processes or to the diffusion of ions in the Helmholtz layer. Moreover, under illumination, the p-Si(100) wafer sample had the smallest arc radius in the low-frequency and high-frequency range indication fast charge transfer and separation due to the formation of the heterojunction. These results are consistent with the research of L.Qiao et al. [30] where the values of R_s and Rct.sc for p-Si wafer were equal 15.83 Ω and132.5Ω, respectively. Fig. 10c shows the Nyquist plot for the p- SiNWs electrode prepared by etching for 30 min in the dark and under solar illumination. Fig. 10d shows a magnification for high-frequency region (0-120 Ω).

The R_s for the p- SiNWs prepared by etching for 15 min was determined to be 23.27Ω. However, the diameter of semicircular arc located at the middle section of z' axis indicates that the electrode charge transfer resistance (Rct) is equal to 72.64 Ω. At low-frequency region, the p- SiNWs electrode prepared with etching time of 15 min was with a smaller semi-circle than that of the n-Si(100) indicating the fast transfer of charges. Moreover, under illumination the p- SiNWs prepared by etching for 15 min showed the smallest arc radius in the low-frequency and high-frequency range indicating the fast charge transfer and separation due to the formation of heterojunction. These results are consistent with that of Qiao et al. who found Rs and Rct.sc for p-SiNWs prepared by Metal catalyzed electroless etching (MCEE) to be equal to 20.38 Ω and123.2 Ω, respectively [30]. Fig. 10e shows the Nyquist plot for the p- SiNWs electrode prepared by etching for 30 min in the dark and under solar illumination. Fig. 10f shows a magnification for the high-frequency region (0-120 Ω). The Rs for the p-SiNWs prepared by etching for 30 min was 25.27Ω. However, the diameter of semicircular arc located at the middle section of z' axis indicates that the electrode charge transfer resistance (Rct) was 69.95 Ω. At low-frequency region, the p-SiNWs electrode prepared with etching time of 30 min was with a smaller semi-circle than that of p-Si(100) indicating fast transfer of charges. Moreover, under illumination p-SiNWs prepared by etching for 30 min showed the smallest arc radius in the low-frequency and high-frequency range indication to the fast charge transfer and separation due to the formation of the heterojunction.
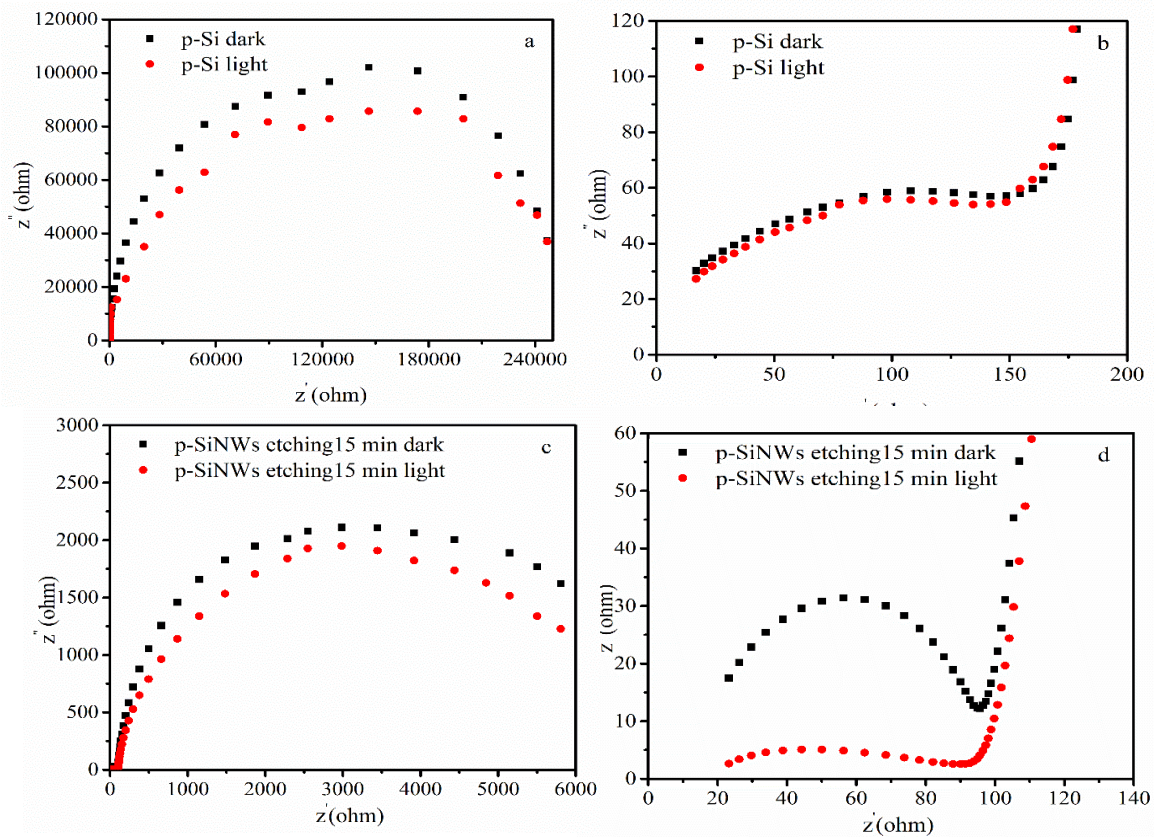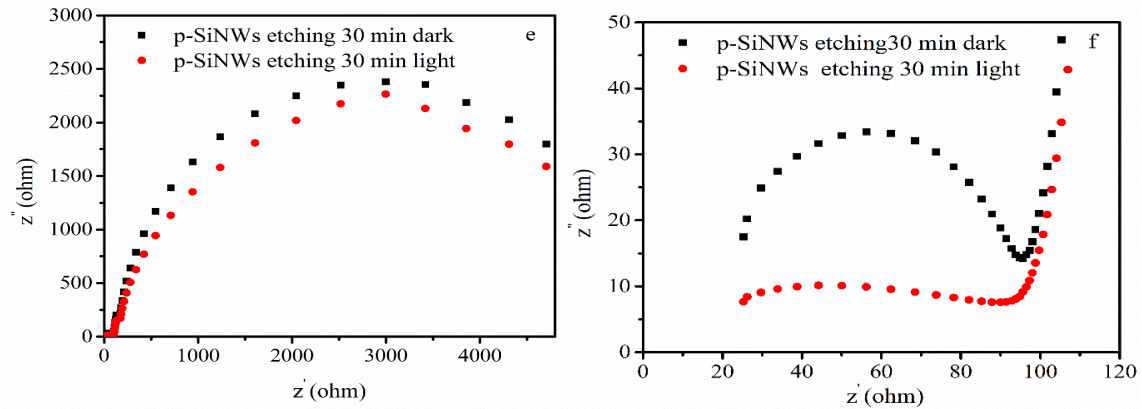
Figure 10: The impedance spectra of (a) p-Si, (b) magnification for high-frequency region for p-Si, (c) p- SiNWs prepared by etching 15 min, (d) magnification for high-frequency region for p-SiNWs prepared by etching 15 min, (e) p- SiNWs prepared by etching 30 min, (f) magnification for high-frequency region for p- SiNWs prepared by etching 30 min.

4. Conclusions

Silicon nanowires (SiNWs) were prepared by the MACE method using an Ag catalyst and different etching times for photoelectrochemical water splitting. The as-prepared SiNWs photocathode by etching for 30 min showed a marked photocurrent density of -0.92 mA cm^{-2} at -1.2 (vs Ag/AgCl) together with photoconversion efficiency(η) of 0.75%. The cyclic voltammetry (CV) measurements under dark were repeated 6 times using different scan rates of 50, 100, 200, 300,400, and 500 mv/s for one cycle. p-Si, p-SiNWs prepared by etching for various times, electrodes exhibited faradaic behavior. Mott–Schottky (M-S) measurements of p-Si(100) wafer and p-SiNWs electrodes prepared by etching for 15 min and 30 min were done using the different frequencies of 100, 1000, and 10000 HZ. Through these measurements, it was observed that the values of VFB were less positive for the prepared SiNWs indicating better performance of the photocathode electrode in capturing and rapidly transferring photogenerated electrons between the semiconductor and electrolyte interfaces. The acceptor density (N$_A$) of photocathodes p-Si (100) wafer and p-SiNWs prepared by etching for 15 min and 30 min at 100 Hz were greater than those at 1000 Hz and 10000 Hz. Results of Nyquist plot were confirmed that all prepared p-SiNWs photocathodes displays two semicircular arcs in the high- and low-frequency regions. At low-frequency region, the p- SiNWs electrode prepared by etching for 30 min was smaller than the of p-Si(100) semi-circle indicating faster transfer of charges. Under illumination, all prepared electrodes showed the smallest arc radius in the low-frequency and high-frequency range indicating fast charge transfer and separation due to the formation of heterojunction.

References

1. Van de Krol R. and Grätzel M., *Photoelectrochemical hydrogen production*. 1 ed. Vol. 90. 2012, New York: Springer.
2. Adib R., Murdock H.E., Appavou F., Brown A., Epp B., Leidreiter A., Lins C., Murdock H., Musolino E., and Petrichenko K., *Renewables 2015 global status report*, in *REN21 Sec. Paris, Fr.* 2015.
3. Lopes T., Andrade L., and Mendes A., *Photoelectrochemical cells for hydrogen production from solar energy*. A.A. Napoleon Enteria (Ed.) Sol. En. Sci. Eng. App, CRC Press Taylor & Francis Group, 2013: pp. 692.

4. Bard A.J. and Fox M.A., *Artificial photosynthesis: Solar splitting of water to Hydrogen and Oxygen.* Accounts of Chem. Res., 1995. **28**(3): pp.141-145.

5. Matsuoka M., Kitano M., Takeuchi M., Tsujimaru K., Anpo M., and Thomas J.M., *Photocatalysis for new energy production: Recent advances in photocatalytic water splitting reactions for Hydrogen production.* Cata. Today, 2007. **122**(1-2): pp.51-61.

6. Gopalakrishnan M., Gopalakrishnan S., Bhalerao G.M., and Jeganathan K., *Multiband InGaN nanowires with enhanced visible photon absorption for efficient photoelectrochemical water splitting.* J. Pow. Sour., 2017. **337**: pp.130-136.

7. Chen Z., Dinh H.N., and Miller E., *Photoelectrochemical water splitting.* Vol. 344. 2013, New York: Springer.

8. Ghosh D., Roy K., Sarkar K., Devi P., and Kumar P., *Surface plasmon-enhanced carbon dot-embellished multifaceted Si (111) nanoheterostructure for photoelectrochemical water splitting.* ACS Appl. Mat. Inter., 2020. **12**(25): pp. 28792-28800.

9. Abe R., *Recent progress on photocatalytic and photoelectrochemical water splitting under visible light irradiation.* J. Photochem. Photobio. C: Photochem. Rev., 2010. **11**(4): pp.179-209.

10. Li Z., Luo W., Zhang M., Feng J., and Zou Z., *Photoelectrochemical cells for solar hydrogen production: current state of promising photoelectrodes, methods to improve their properties, and outlook.* En. Envi. Sci., 2013. **6**(2): pp. 347-370.

11. Abdulelah H., Ali B., Mahdi M.A., Hassan J.J., Al-Taay H.F., and Jennings P., *Fabrication and characterization of nanowalls CdS/dye sensitized solar cells.* Phys. E: L.-dimen. Sys. Nanos., 2017. **90**: pp. 104-108.

12. Kadhim M.J., Mahdi M.A., Hassan J.J., and Al-Asadi A.S., *Photocatalytic activity and photoelectrochemical properties of Ag/ZnO core/shell nanorods under low-intensity white light irradiation.* Nanotech., 2021. **32**(19): pp.195706.

13. Bashkany Z.A., Abbas I.K., Mahdi M.A., Al-Taay H.F., and Jennings P., *A self-powered heterojunction photodetector based on a PbS nanostructure grown on porous silicon substrate.* Silicon, 2018. **10**(2): pp.403-411.

14. Mahdi M.A., Abdul-Hameed A., Ali B., and Al-Taay H.F., *Fabrication of SiNWs/PEDOT: PSS heterojunction solar cells.* Ir. J. Mat. Sci. Eng., 2020. **17**(1): pp.69-76.

15. Li X., *Electroless etched silicon nanostructures for solar energy conversion*, Thesis, Halle (Saale), Universitäts-und Landesbibliothek Sachsen-Anhalt, Diss., 2013.

16. Chen Z., Ning M., Ma G., Meng Q., Zhang Y., Gao J., Jin M., Chen Z., Yuan M., and Wang X., *Effective silicon nanowire arrays/WO3 core/shell photoelectrode for neutral pH water splitting.* Nanotech., 2017. **28**(27): pp.275401(1-9).

17. Chunqian Z., Chuanbo L., and Zhi L., *Enhanced photoluminescence from porous Silicon nanowire arrays [J].* Nano. Res. Lett., 2013. **8**: pp.277(1-4).

18. Cardon F. and Gomes W.P., *On the determination of the flat-band potential of a semiconductor in contact with a metal or an electrolyte from the Mott-Schottky plot.* J. Phys. D: Appl. Phys., 1978. **11**(4): pp. L(63-67).

19. Xin C., Wang Y., Zhang S., Xu L., Yu Y., Xiang H., Wu W., and Hua J., *Energy band transition and voltage compensation via surface stoichiometry alteration in p-type dye-sensitized solar cells.* Phys. Stat. Sol. –Rap. Res. Lett., 2017. **11**(10): pp. 700258(1-6).

20. Wang L.C., De Tacconi N.R., Chenthamarakshan C.R., Rajeshwar K., and Tao M., *Electrodeposited copper oxide films: Effect of bath pH on grain orientation*

and orientation-dependent interfacial behavior. Th. Sol. Fil., 2007. **515**(5): pp. 3090-3095.

21. Rai S., Bhujel R., Mondal M.K., Swain B.P., and Biswas J., *Study of the morphological, optical, structural and electrical properties of Silicon nanowires at varying concentrations of the catalyst precursor.* Mat. Advan., 2022. **3**(6): pp. 2779-2785.

22. Sim U., Jeong H.-Y., Yang T.-Y., and Nam K.T., *Nanostructural dependence of hydrogen production in silicon photocathodes.* J. Matt. Chem. A, 2013. **1**(17): pp. 5414-5422.

23. Sim Y., John J., Moon J., and Sim U.K., *Photo-assisted hydrogen evolution with reduced graphene oxide catalyst on silicon nanowire photocathode.* Appl. Sci., 2018. **8**(11): pp.2046(1-12).

24. Wu C., Yin M., Zhang R., Li Z., Zou Z., and Li Z., *Further studies of photodegradation and photocatalytic Hydrogen production over Nafion-coated Pt/P25 sensitized by Rhodamine B.* Int. J. Hyd. En., 2020. **45**(43): pp.22700-22710.

25. Ali A.A., Nazeer A.A., Madkour M., Bumajdad A., and Al Sagheer F., *Novel supercapacitor electrodes based semiconductor nanoheterostructure of CdS/rGO/CeO₂ as efficient candidates.* Ar. J. chem., 2018. **11**(5): pp.692-699.

26. Kumar S., Aziz S.K.S., Kumar S., Riyajuddin S.K., Yaniv G., Meshi L., Nessim G.D., and Ghosh K., *Three-dimensional graphene-decorated copper-phosphide (Cu3P@ 3DG) heterostructure as an effective electrode for a supercapacitor.* Fron. Mat., 2020. **7**: pp.30(1-11).

27. Qi H., Bo Z., Yang S., Duan L., Yang H., Yan J., Cen K., and Ostrikov K.K., *Hierarchical nanocarbon-MnO₂ electrodes for enhanced electrochemical capacitor performance.* En. Stor. Mat., 2019. **16**: pp. 607-618.

28. Song B., Wang X., Xin C., Zhang L., Song B., Zhang Y., Wang Y., Wang J., Liu Z., and Sui Y., *Multiferroic properties of Ba/Ni co-doped KNbO₃ with narrow band-gap.* J. All. Comp., 2017. **703**: pp.67-72.

29. Meng H., Fan K., Low J., and Yu J., *Electrochemically reduced graphene oxide on silicon nanowire arrays for enhanced photoelectrochemical Hydrogen evolution.* Dalt. Trans., 2016. **45**(35): pp.13717-13725.

30. Qiao L., Liao M., Fang K., He X., and Zhang Y., *Enhancement of photoelectrochemical Hydrogen evolution of p-type silicon nanowires array by loading MoS₂.* Silicon, 2019. **11**(4): pp.1963-1970.

31. Joe J., Yang H., Bae C., and Shin H., *Metal chalcogenides on silicon photocathodes for efficient water splitting: A mini overview.* Catalysts, 2019. **9**(2): pp.149(1-37).

32. Ramadan R. and Martín-Palma R.J., *Electrical characterization of MIS Schottky barrier diodes based on nanostructured porous Silicon and Silver nanoparticles with applications in solar cells.* Energies, 2020. **13**(9): pp.2165(1-15).

33. Riveros G., León M., and Ramírez D., *Effect of chloride ions on the structural, optical, morphological, and electrochemical properties of Cu₂O films electrodeposited on Fluorine-doped tin Oxide substrate from a DMSO solution.* J. Chil. Chem. Soci., 2016. **61**(4): pp.3219-3223.

تحضير فوتوكاثود أسلاك السيليكون النانوية لتقسيم المياه الكهروكيميائية الضوئية

زينب كاظم علي[1] و مازن عوني مهدي[1]

[1]قسم الفيزياء، كلية العلوم، جامعة البصرة، العراق

الملخص

تم استخدام عملية الحفر الكيميائي بمساعدة المعدن والتي تستخدم رقائق السيليكون من النوع p مع فترات حفر متنوعة لإنتاج أسلاك السيليكون النانوية. تُستخدم الجسيمات النانوية الفضية المحضرة بالترسيب الكيميائي كعامل مساعد في تكوين أسلاك السيليكون النانوية. أكدت الصور المأخوذة من الفحص المجهري الإلكتروني للانبعاثات الميدانية أن قطر SiNWs ينمو عندما تزداد مدة الحفر. تم فحص خصائص الخلية الكهروكيميائية الضوئية باستخدام أسلاك السيليكون كأقطاب كهربائية عاملة. اكدت قياسات قياس الجهد الكهربي الخطي (JV) على p-SiNWs أن كثافة التيار الضوئي ارتفعت من 0.20 مللي أمبير سم $^{-2}$ إلى 0.92 مللي أمبير سم 2 حيث زادت مدة الحفر لـ SINWs المحضرة من 15 إلى 30 دقيقة. كانت كفاءة التحويل (η) 0.47 لـ p-SiNWs المحضرة بوقت حفر مدته 15 دقيقة و0.75 لـ p-SiNWs المحضرة بوقت نقش مدته 30 دقيقة. أثبتت تجارب قياس الجهد الدوري (CV) التي أجريت بمعدلات مسح مختلفة صحة السلوك الفارادي لـ p-SiNWS المحضر لمدة 15 و30 دقيقة من الحفر. بسبب الانتشار البطيء للأيونات وزيادة معدل المسح، انخفضت السعة بزيادة معدل المسح. أظهر تحقيق (M-S) Mott-Schottky تركيزًا كبيرًا للحاملات بمقدار 3.66 × 10^{20} سم $^{-3}$. وفقًا لنتائج التحليل الطيفي للمقاومة الكهروكيميائية(EIS) ، فإن الكاثود الضوئي SiNWs الذي تم تحضيره بالحفر لمدة 30 دقيقة كان له مقاومة نقل شحنة تبلغ 25.27Ω ، وهو منخفض بدرجة كافية لتعزيز نقل الشحنة البينية.